Molecular imaging with reporter genes: Brader and colleagues offer perspectives on radionuclide-based reporter gene imaging as developed and applied in preclinical and clinical studies . . . . . ***Page 167***

^{18}F^{-}/^{18}F-FDG PET/CT: Cook previews an article in this issue of *JNM* on the effectiveness of coinjection of these tracers in PET/CT imaging of patients with cancer and possible skeletal metastases . . . . . ***Page 173***

^{18}F-fluoride and ^{18}F-FDG PET/CT: Iagaru and colleagues report on the use of combined ^{18}F^{-}/^{18}F-FDG in a single PET/CT examination for evaluation of cancer patients and compare the results with those from separate ^{18}F^{-} and ^{18}F-FDG PET/CT imaging. . . . . ***Page 176***

PET in primary CNS lymphoma: Kasenda and colleagues investigate the prognostic utility of pretreatment ^{18}F-FDG PET in patients with primary central nervous system lymphoma . . . . . ***Page 184***

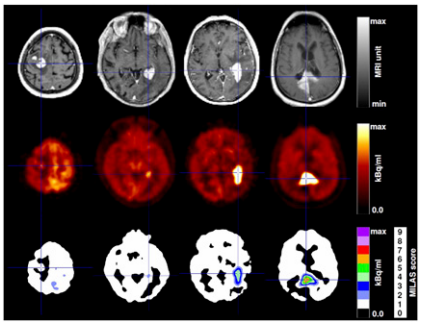

Dual-tracer PET/CT and liver transplantation: Cheung and colleagues compare the effectiveness of ^{11}C-acetate and ^{18}F-FDG PET/CT with that of contrast CT in selecting patients with hepatocellular carcinoma for liver transplantation on the basis of the Milan criteria . ***Page 192***

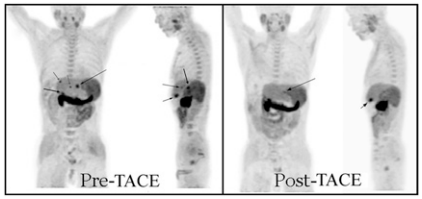

^{18}F-FMISO PET reproducibility: Okamoto and colleagues assess the reproducibility of tumor hypoxia by using quantitative analysis of ^{18}F-FMISO uptake in patients with untreated head and neck cancer . . . . . ***Page 201***

Visualization of brown adipose tissue: Admiraal and colleagues look at the feasibility of and incremental information provided by combined ^{123}I-MIBG SPECT/CT and ^{18}F-FDG PET/CT imaging of brown adipose tissue activity in humans during cold exposure. . . . . ***Page 208***

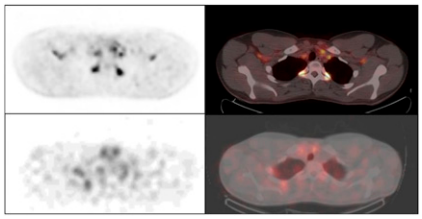

^{11}C-PIB PET and cardiac amyloid: Antoni and colleagues explore the use of ^{11}C-PIB PET as a specific diagnostic for cardiac amyloidosis in patients with systemic amyloidosis. . . . . ***Page 213***

Fully automated cardiac SPECT: Arsanjani and colleagues compare the performance of fully automated quantification of attenuation-corrected and noncorrected myocardial perfusion SPECT with the corresponding performance of experienced readers in detection of coronary artery disease. . . . . ***Page 221***

^{18}F-FET PET in cerebral lesions: Rapp and colleagues assess the clinical value of ^{18}F-FET PET in the initial diagnosis of cerebral lesions suggestive of glioma. . . . . ***Page 229***

Tissue density and 3D dosimetry: Dieudonné and colleagues evaluate the impact of tissue density heterogeneities on dosimetry when using a dose kernel convolution method in absorbed dose calculations in molecular radionuclide therapy and propose a density correction method. . . . . ***Page 236***

^{18}F-labeled agent for islet imaging: Wu and colleagues describe the development of and initial studies with an ^{18}F-labeled exendin-4 PET agent with high specific activity for islet imaging targeting the glucagonlike peptide-1 receptor . . . . . ***Page 244***

Metformin and tumor metabolism: Habibollahi and colleagues investigate this antidiabetes drug as a central cellular energy sensor and explore the effects on glucose uptake as well as on ^{18}F-FDG and ^{18}F-FLT PET in assessing its effectiveness as an antineoplastic agent . . . . ***Page 252***

Metformin and gut metabolism: Massollo and colleagues conduct animal studies designed to explain the mechanisms that result in high bowel radioactivity in ^{18}F-FDG PET staging of abdominal cancer lesions in patients on metformin treatment . . . . . ***Page 259***

PET for functional analysis of BCRP: Takashima and colleagues describe a quantitative ^{11}C-labeled PET method for assessing hepatobiliary and renal excretion of a breast cancer resistance protein substrate in mice . . . . . ***Page 267***

Cardiac endothelin receptor PET: Higuchi and colleagues determine the feasibility

of using an ^{18}F-labeled ligand for imaging the endothelin subtype-A receptor in healthy and injured rat heart . . . . . ***Page 277***

^{15}O gas PET in rats: Watabe and colleagues detail the use of the ^{15}O gas steady-state inhalation method for normal anesthetized rats and resulting PET assessments of cerebral blood flow, cerebral metabolic rate, oxygen extraction fraction, and cerebral blood volume . . . . . ***Page 283***

PET and TSPO in EAE: Mattner and colleagues use ^{18}F-PBR111, with high affinity and selectivity for the translocator protein, in a small-animal PET investigation of neuroinflammation at different phases of relapsing–remitting experimental autoimmune encephalomyelitis . . . . . ***Page 291***

Synthesis and evaluation of ^{18}F-FE-PEO: Riss and colleagues describe the development of and early studies with this ^{18}F-labeled opioid receptor agonist as a candidate PET tracer with specific advantages over ^{11}C-labeled agonist radiotracers in the brain . . . . . ***Page 299***

Simultaneous submillimeter SPECT and PET: Goorden and colleagues introduce a versatile-emission CT system for radionuclides that enables simultaneous submillimeter imaging of single-photon and positron-emitting radiolabeled molecules . . . . . ***Page 306***

Future of ^{99m}Tc: Pillai and colleagues discuss strategies to sustain the availability of ^{99m}Tc without the use of highly enriched uranium, as well as scientific, economic, and other factors likely to affect medical access to this vital molecular imaging component . . . . . ***Page 313***

ON THE COVER

^{11}C-PIB PET has shown promise in the specific identification of cardiac amyloid deposits. Uptake is obvious in the left ventricular wall of patients.

See page 213.